NANO LETTERS

pubs.acs.org/NanoLett Letter

Optically Driven Gold Nanoparticles Seed Surface Bubble Nucleation in Plasmonic Suspension

Qiushi Zhang, Ruiyang Li, Eungkyu Lee,* and Tengfei Luo*

Cite This: https://doi.org/10.1021/acs.nanolett.0c04913 Read Online

ACCESS | Metrics & More | Article Recommendations | Supporting Information

ABSTRACT: Photothermal surface bubbles play important roles in applications like microfluidics and biosensing, but their formation on transparent substrates immersed in a plasmonic nanoparticle (NP) suspension has an unknown origin. Here, we reveal NPs deposited on the transparent substrate by optical forces are responsible for the nucleation of such photothermal surface bubbles. We show the surface bubble formation is always preceded by the optically driven NPs moving toward and deposited to the surface. Interestingly, such optically driven motion can happen both along and against the photon stream. The laser power density thresholds to form a surface bubble drastically differ depending on if the surface is forward- or backward-facing the light propagation direction. We attributed this to different optical power densities needed to enable optical pulling and pushing of NPs in the suspension, as optical pulling requires higher light intensity to excite supercavitation around NPs to enable proper optical configuration.

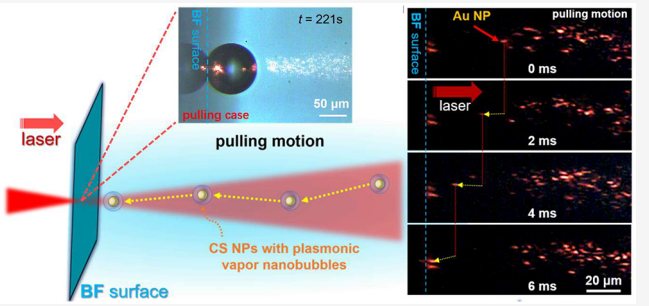

KEYWORDS: *gold nanoparticles, plasmonic heating, microbubble dynamics, optical force*

INTRODUCTION

Surface bubbles generated by photothermal effects are playing significant roles in a wide range of applications, such as microbubble logics,[1] vapor generation,[2−4] cancer therapy,[5−9] plasmon-assisted catalysis,[10−13] and nanoparticle (NP) manipulation[14−18] and deposition.[19−21] To realize the photothermal effect, a light-absorbing substrate, such as silicon, thin-metallic layer, and conducting oxide, is usually immersed in liquid to convert optical energy into thermal energy.[15,16,19] When the light intensity is sufficiently high to raise the temperature of the substrate above a threshold, a surface bubble can nucleate.

For photothermal conversion, metallic nanostructures are among the most efficient transducers, as they can support the surface plasmonic resonance to amplify the light intensity at the metal/dielectric interface by orders of magnitude.[22,23] In addition, since the resonant wavelength of the surface plasmonic resonance can be tuned by properly designing the shape, spacing, and size of the metallic nanostructures at the subwavelength scale, there have been systematic studies of surface bubble formation with surface plasmonic resonance (i.e., plasmonic surface bubble).[11,24−30] Fundamental studies have focused on the growth dynamics of the plasmonic surface bubbles, revealing interesting physics about bubble oscillation, vaporization, and gas expelling.[31,32] With well-defined surface photothermal heat flux, bubble nucleation time is found to be inversely proportional to the concentration of dissolved air in liquid.[31,33,34] On the periodic metal nanostructures (i.e., pillar or cylinder), it is observed that the laser power density threshold for bubble nucleation depends on the number density of the nanostructures.[28,35] Overall, it has been known that the photothermal bubble generation process at a surface with plasmonic nanostructures is in principle similar to the conventional pool boiling, where the predecorated substrate is working as a heat source, as well as providing nucleation sites for bubble nucleation.[11,28,31−34,36−41]

However, it has been reported that surface bubble can be generated on optically transparent substrates when it is immersed in plasmonic NP suspensions.[20,21,30,42] While the plasmonic NPs suspending in liquid can heat up the irradiated volume of liquid when illuminated by a resonant light, there are no light-absorbing materials on the surface that convert optical energy into surface heating. The fundamental question here is how surface bubbles can be formed with the absence of direct surface heating source? In this work, we investigate the origin of surface bubble generation in plasmonic NP suspension on the transparent substrate. High-speed videography reveals that the light-guided NP deposition on the surface is a necessity for bubble nucleation, and it is the scattering optical pulling/pushing force that drives such

Received: December 14, 2020
Revised: April 28, 2021

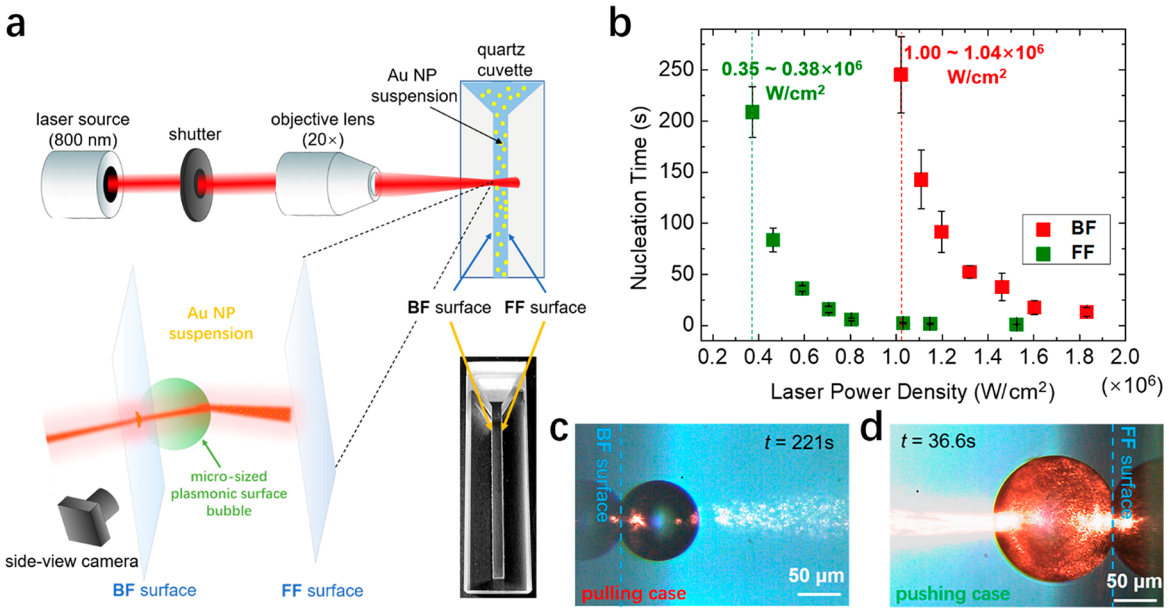

Figure 1. (a) Schematic of the experimental setup to characterize the surface bubble nucleation on the backward-facing (BF) or the forward-facing (FF) surface with respect to the laser propagating direction. (b) Nucleation time of surface bubble on the BF or FF surface as a function of the laser power density. The laser power density thresholds of the two cases are identified with vertical lines. (c and d) Representative optical images of nucleated surface bubble on (c) the BF surface and (d) the FF surface.

deposition. Interestingly, the thresholds of laser power density to form a surface bubble by optical pulling force is much higher than the pushing force due to that a supercavitating nanobubble around the NP is required for optical pulling to happen.[43] These results reveal interesting physics leading to photothermal surface bubble generation in NP suspensions.

RESULTS AND DISCUSSION

We first demonstrate that surface bubbles can be generated in the core−shell (CS) NP suspension (concentration ~ 2×10^{15} particles/m^3) when the laser at the wavelength of surface plasmonic resonance peak is focused on either the backward-facing (BF) or the forward-facing (FF) surface with the optical system[29,30] shown in Figure 1a (see Supporting Information, SI1, for details of experiments, and Supporting Movies M1 and M2 for observations). To shed light on the mechanism of bubble formation, we investigated the nucleation time as a function of laser power density. The laser power density we refer to in this work is the maximum of laser power density at the center of the Gaussian beam for a given laser power. We note that the nucleation time in this study is defined as the time between the moment of turning on the laser and the onset of nucleation. In the experiments, the onset of surface bubble nucleation can be identified by observing the strongly scattered light at the surface where the laser beam is focused on (see Supporting Information, SI2). We note that the surface bubble nucleation in NP suspension includes a NP deposition stage after turning on the laser as discussed later. As a result, the time interval between turning on the laser and the observation of the strongly scattered light is the total time including NP deposition and the nucleation of a surface bubble. We also note that how bubble nucleation time is defined may vary in different context. For example, on prefabricated plasmonic substrates,[31,34] the nucleation time is the interval between switching on the laser and the onset of a giant vapor bubble. In these cases, the giant bubble collapses within ~200 μs, followed by a subsequent oscillating bubble lasting for <2000 μs, which precedes the emergence of a stably growing vapor bubble. Since our measured nucleation times are on the order of 1−100 s, whether the onset of nucleation is chosen to be the start of the initial giant bubble or the subsequent stable bubble does not influence our analyses.

Our measurements show that the nucleation time can be shortened as the laser power density increases (Figure 1b). At the same time, however, it is found that at a certain power density, the nucleation times of bubbles on the FF surface are always shorter than those on the BF surface. We have also noticed that the thresholds of the power density to form a surface bubble in each of the two cases are drastically different. For nucleation on the FF surface, the threshold is $0.35-0.38 \times 10^6$ W/cm^2, but for the BF surface, the threshold is much higher, $1.00-1.04 \times 10^6$ W/cm^2.

One mechanism that can potentially contribute to the surface bubble formation in the NP suspension is volumetric photothermal heating,[29] where the CS NPs in suspension absorb laser energy and heat up the laser-irradiated volume. However, if the bubble formation is such a purely thermal process, the nucleation dynamics would be similar for both the BF and FF surfaces when the laser is focused on them, respectively. Furthermore, if the surface bubble nucleation depends on the local temperature of the surface, as that in pool boiling, the threshold of laser power density for the bubble nucleation on the FF surface would be higher than that on the BF surface, since the laser energy is attenuated by the light-absorbing NPs in suspension while reaching the FF surface (see Supporting Information, SI3, for modeling details). Thus, the photothermal volumetric heating cannot explain the observed discrepancy in nucleation times on the BF and FF surfaces.

Upon detailed analysis of the side view high-speed videography, we observe that there are always CS NPs moving toward the surfaces leading up to every bubble nucleation (Figures 2a and b, Supporting Movies M3 and M4). In the experiments, we track the positions of the glowing dots as a

https://doi.org/10.1021/acs.nanolett.0c04913
Nano Lett. XXXX, XXX, XXX−XXX

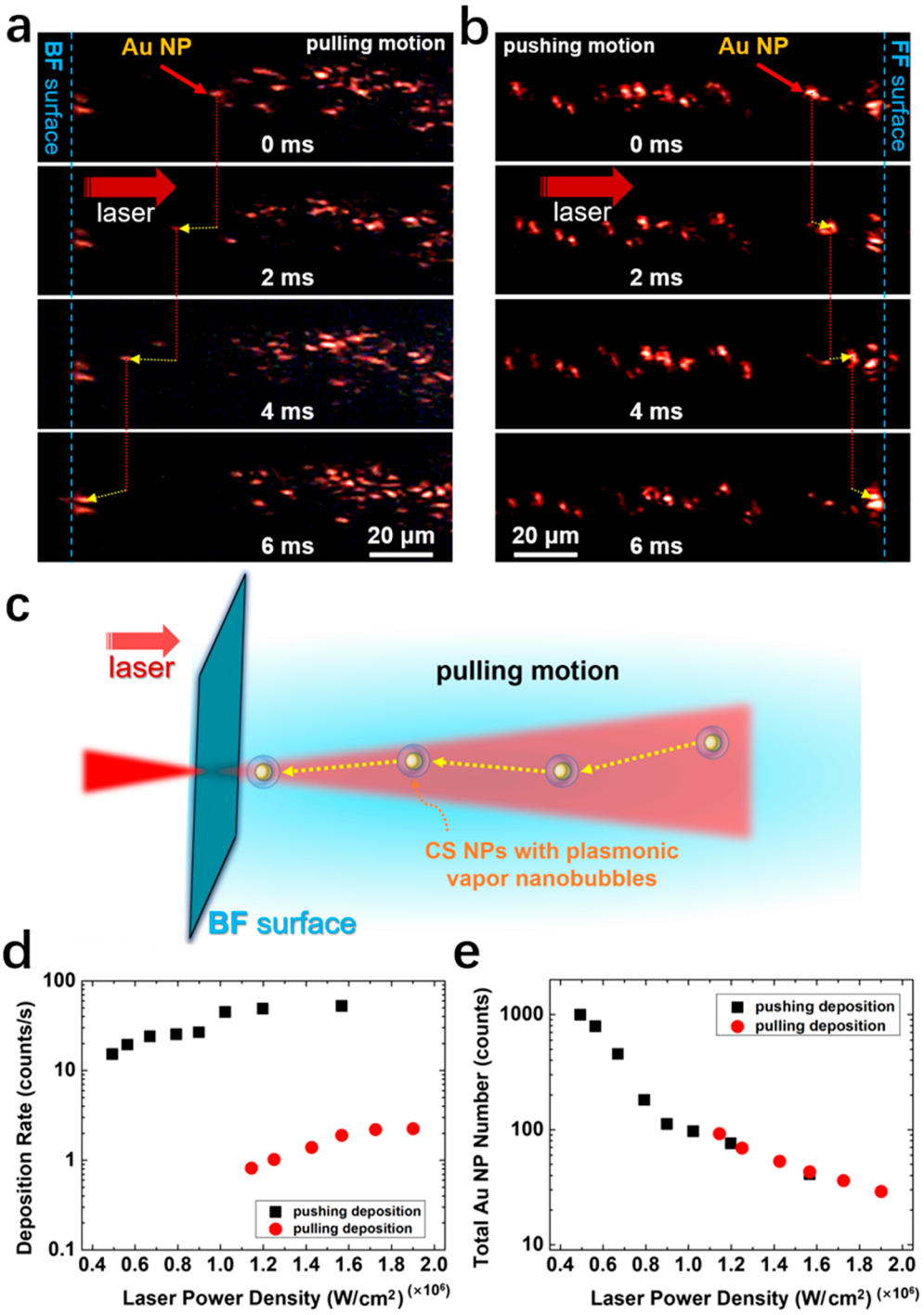

Figure 2. (a and b) Dark field optical images of optically driven CS NPs moving (a) against the light propagation direction by optical pulling force, and (b) along the light propagation direction by optical pushing force, as a function of time. The moving NPs are indicated by red arrows, and the yellow arrows show the trajectory of the NP between two frames. (c) Schematic of a supercavitating CS NP that has an optical condition enabling optical pulling motion.[43,44] (d) Deposition rate of CS NP and (e) the average total number of CS NP deposited on surface prior to surface bubble nucleation as a function of the laser power density.

function of time. As shown in the scanning electron microscope image in our previous work, ref 44, these CS NPs are deposited as isolated single NPs on the surface, which excludes the possibility of aggregated NPs during their motions. Therefore, one glowing dot corresponds to the diffraction-limited scattered spot from a single CS NP in the side view high-speed videography. When the laser power density is low (<0.35 × 10^6 W/cm^2), such NP motion along the laser beam axis is not apparent, and there is no bubble formation. When the laser is focused on the FF surface, NPs moving toward the surface is observed when the laser power density is above 0.35−0.38 × 10^6 W/cm^2, and bubble nucleation follows. When the laser is focused on the BF surface, there are NPs moving toward the surface only if the laser power density is above 1.00−1.04 × 10^6 W/cm^2, following which bubble nucleation is also observed. Such NP

https://doi.org/10.1021/acs.nanolett.0c04913
Nano Lett. XXXX, XXX, XXX−XXX

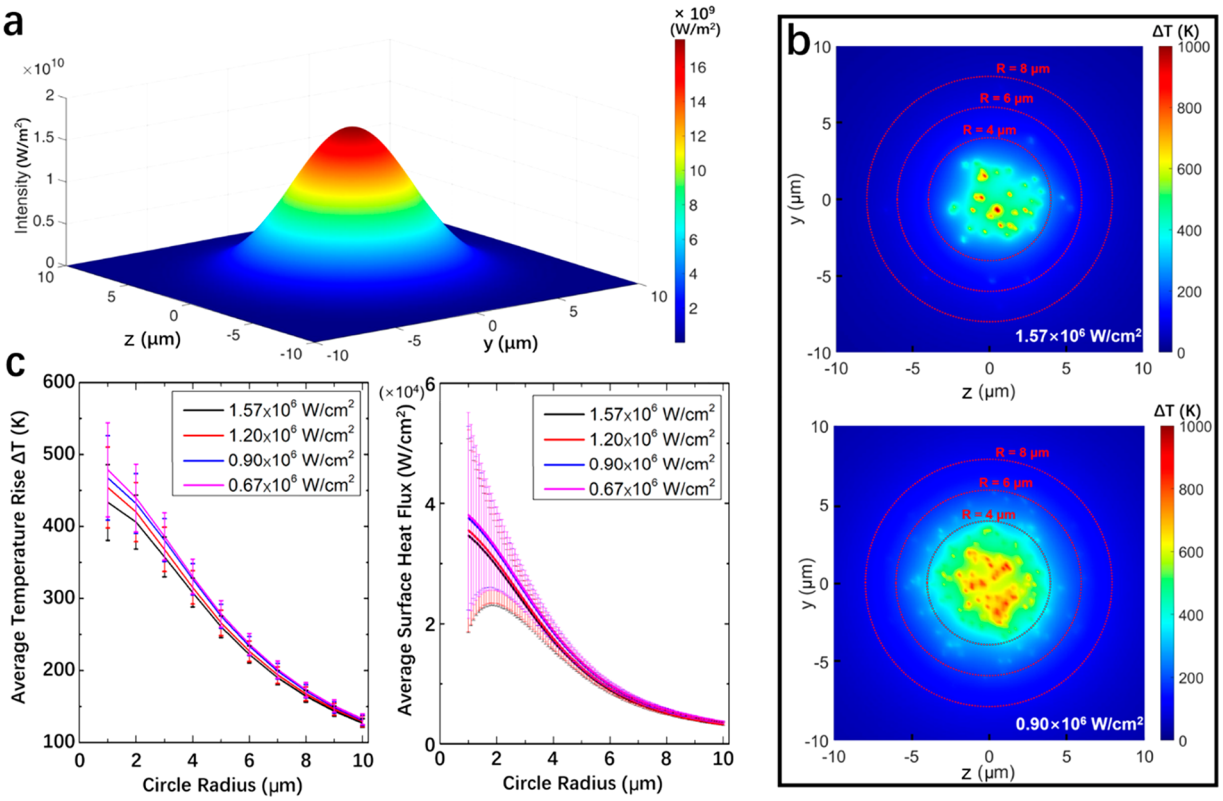

Figure 3. (a) Simulated incident laser power density profile, with the laser power density of 1.76×10^6 W/cm^2 (corresponds to the laser power of 1W). (b) Calculated surface temperature rise (from room temperature) profiles in the NP deposition area under the laser power densities of (top panel) 1.57×10^6 W/cm^2 (corresponds to the laser power of 890 mW), and (bottom panel) 0.90×10^6 W/cm^2 (corresponds to the laser power of 510 mW). (c) Left panel: Average surface temperature rise (with respect to room temperature). Right panel: Average surface heat flux of the NP deposition area with different radii from laser beam center under different laser power densities. The circular area radii equal to 4, 6, and 8 μm are depicted in panel b.

movements along the laser beam propagation direction are observed within ~50 μm from the surfaces, and they cannot be driven by thermal convective flow, since it is vertical near the walls of the upright cuvette (see Supporting Information, Figure S3). These, thus, show that NP moving toward the focused surface is a necessity for surface bubble nucleation. Then the question is what drives such NP movements?

Our previous studies have found that CS NPs in a suspension can be driven by scattering optical force originated from the momentum exchange between incident photons and the NPs.[43−45] The photon stream in the laser beam usually exerts an optical pushing force that drives the CS NPs to move in the light propagating direction. However, as reported in several previous works,[44,46−52] plasmonic vapor nanobubbles can be formed around the heated CS NPs irradiated by a pulsed laser at the surface plasmonic resonance peak of the NPs. This supercavitation (i.e., nanobubble encapsulating the NP) can optically couple to the encapsulated NP to trigger the "negative" scattering optical forces on the NP, leading to an optical pulling force (Figure 2c), depending on the position of a CS NP inside the nanobubble.[43−45] The initial location of CS NP inside nanobubble is stochastic because of Brownian motion,[45] as well as the stochastic nature of nanobubble dynamics (nucleation and growth). As a result, only a portion of the NPs which have locations inside the nanobubble favoring negative optical force can achieve negative motion, as discussed in detail in refs 43 and 44. In these conditions, the laser beam can drive the CS NP to move against the photo stream, and this is why some NPs are seen moving against the light propagation direction toward the BF surface. We note, as discussed in ref 44, since the supercavitating CS NP, which is intensely heated by laser, can evaporate the liquid instantaneously during its motion to ensure that the NP is always encapsulated in the vapor phase, the Marangoni stresses at liquid−vapor interface is not important in influencing the relative position of NP in nanobubble. Since such supercavitation needs relatively high laser power density to intensely heat the NP, the pulling motion is not observed until a laser power density threshold is reached. It is worth noting that the fluence to create the supercavitating nanobubble for the CS NP used in this work has been known to be ~7 mJ/cm^2,[50] which is close to the threshold of the laser power density ($1.00−1.04 \times 10^6$ W/cm^2, converted to fluence is 7.4−7.7 mJ/cm^2) to form the bubble on the BF surface. We also note that once the threshold is met, the generated nanobubble size does not change much as a function of NP temperature,[45] suggesting that different laser powers will not significantly change the probability of achieving optical pulling forces. On the contrary, the CS NPs driven by the optical pushing force can occur without the need of supercavitation. Therefore, we see plenty of NPs moving toward the FF surface even with a laser power density of 0.37×10^6 W/cm^2. These facts lead us to believe that it is such optical forces that drive the NPs to be deposited on the surfaces, which then serve as the heating source on the surface for bubble nucleation.

https://doi.org/10.1021/acs.nanolett.0c04913
Nano Lett. XXXX, XXX, XXX−XXX

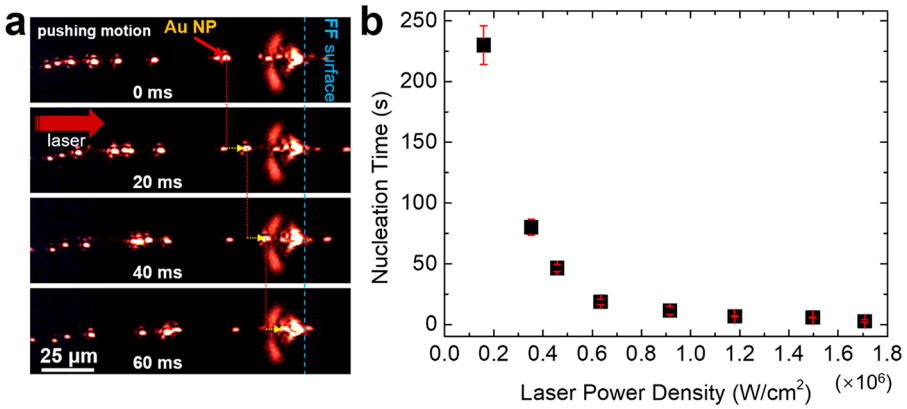

Figure 4. (a) Optical images of the optical pushing motion of a solid spherical Au NP indicated by the red arrow. The focal plane of the laser is on the FF surface. The time interval between each image is 20 ms. (b) Surface bubble nucleation time as a function of laser power density in the pushing case of solid spherical Au NP.

To quantitatively investigate the relationship between the optically driven CS NPs and the surface bubble formation, we analyze the number of CS NPs moving toward and reaching each surface prior to bubble nucleation with the high-speed videography. It is found that the number of CS NP deposited on the BF surface per unit time (i.e., deposition rate) is 1 order of magnitude lower than that on the FF surface (see Figure 2d). This observation is reasonable as enabling the optical pulling of a CS NP requires the presence of a encapsulating nanobubble, and even with the supercavitation, the NP can only experience optical pulling force when it is in a certain region inside the nanobubble as previously studied in ref.[44] This is in sharp contrast to the cases of optical pushing motion that happens without the need of supercavitation. As a result, there is a higher possibility that CS NPs undergo pushing motion than pulling motion under laser irradiation, which leads to the higher NP deposition rates on the FF surface. Interestingly, the accumulated numbers of CS NPs deposited on the BF and FF surfaces prior to bubble nucleation are almost the same for a certain power density range (Figure 2e). This strongly indicates that the bubble nucleation is due to the surface heating provided by the deposited NPs via the photothermal energy conversion. It also suggests that the surface temperature history is not important to nucleation, but it is the instantaneous photothermal heat flux and the local temperature profile when sufficient NPs are deposited on surface that trigger the bubble nucleation.

To investigate the thermal threshold to enable bubble nucleation, we study the average surface temperature rise from room temperature and heat flux of the area enclosing the deposited NPs under a Gaussian laser beam irradiation (Figure 3a) using Monte Carlo simulations. The details of the simulation can be found in the Supporting Information, SI4. As shown in our previous work ref 44, the NPs are deposited as isolated single NPs on the surface. In addition, based on the simulations in our previous work,[30] the optical hybridization of these Au NPs, if any, does not significantly influence the heating efficiency. Thus, in the simulation, the NPs are modeled as single isolated ones. Taking the experimentally measured numbers of deposited NPs prior to surface bubble nucleation (Figure 2e) as the inputs, the Monte Carlo simulation is used to produce 100 independent configurations of randomly deposited NPs for each laser power density. For each configuration, the resultant surface temperature profile and heat flux for this laser power are calculated. At the power density between 0.67×10^6 and 1.57×10^6 W/cm^2, it is found that there can be local hot spots with temperatures rise up to ~1000 K, if multiple NPs are closely deposited (see Figure 3b). However, we believe the observed bubble nucleation is not driven by these hot spots, which strongly depends on the configuration of deposited NPs, since the numbers of deposited NPs in each of the five runs of the same experiment do not differ more than 10%. On the other hand, when we pick five random configurations from the Monte Carlo simulation, the chance to obtain such hot spots is very small. In another word, the emergence of the hot spot strongly depends on the spatial distribution of the deposited NPs. As a result, we believe the bubble nucleation we observed is more related to the average thermal condition of the surface.

We, then, investigate the average surface temperature and heat flux in circular areas with different radii, as shown in Figure 3c. The areas are defined as the circles centered at the origin of the Gaussian beam profile (Figure 3b). Both the calculated average temperature profiles and heat flux are within the error bars of each other for different laser power densities, and as the circle radius increases, the average temperature and heat flux from different laser power densities further converge. As seen in Figure 3c, the average surface temperature decreases as the surface area increases for any power densities. It was reported in ref 31 that the critical nucleation temperature of surface bubble on predeposited plasmonic surfaces is ~422 K in gas-rich deionized water, which is very similar to our case. In addition, ref 31 also showed that the diameter of a so-called giant bubble, based on which nucleation was defined, is 10−20 μm in diameter. In Figure 3c, we can see that the average surface temperature above 422 K would be from a radius of 9−10 μm (i.e., a diameter of 18−20 μm), that is similar to the size of the reported giant bubble. This at least supports that the experimentally determined critical number of deposited NPs prior to bubble nucleation can lead to the surface temperatures high enough to form a surface bubble. These findings also indicate that it is the surface heating effect from the deposited NP that leads to the surface bubble nucleation in a NP suspension. For a given laser power density, it is necessary to accumulate sufficient NPs on the surface to reach the nucleation temperature before a surface bubble can be formed. When the laser power density is lower, more NPs need to be deposited to convert the laser energy into heat to raise the temperature to the critical value for bubble nucleation, and

https://doi.org/10.1021/acs.nanolett.0c04913
Nano Lett. XXXX, XXX, XXX−XXX

when the laser power density is higher, less NPs need to be deposited to reach the same effect.

As a comparison, we also studied surface bubble nucleation in a suspension of solid Au NP. Each of the spherical solid Au NP has a diameter of 103 ± 10 nm. The concentration of the solid Au NPs is ~4.3×10^{15} particles/m^3, and the dissolved air level is the same as the CS Au NPs suspension (i.e., air equilibrium). The higher concentration of this solid Au NP suspension than the previous CS Au NP suspension (~2.0×10^{15} particles/m^3)can avoid extremely long nucleation time which may cause significant error in the results. We first focus the laser on the BF surface, but we cannot observe any pulling motion of the solid Au NPs or bubble nucleation even the laser power density is increased to 1.85×10^6 W/cm^2, the maximum achievable in our experimental setup (Supporting Movies M5). Because of the mismatch between the surface plasmonic resonance wavelength of the solid Au NP (563 nm) and the incident laser wavelength (800 nm), there is no significant plasmonic heating effect, and thus, it is very difficult for the NP to form supercavitation, which is essential for achieving the optical pulling effect.[43,44] However, we can still see robust optical pushing motion of NPs when the laser focal plane is on the FF surface (Figure 4a, Supporting Movie M6). This pushing motion again results in the deposition of NPs on the surface, and thus, surface bubbles can still be formed and grow under the irradiation of the off-surface plasmonic resonance laser beam (Supporting Movie M6). The bubble nucleation time as a function of laser power density is plotted in Figure 4b. This experiment further confirms that the NP deposition is a necessity for photothermal surface bubble formation in plasmonic NP suspensions.

CONCLUSIONS

In conclusion, we have elucidated the mechanism of surface bubble formation on a transparent bare quartz surface immersed in plasmonic CS or solid Au NP suspension. The forward- or backward-moving NPs driven by optical pushing or pulling force can be deposited on the surface and then act as surface photothermal plasmonic heaters on the transparent substrate. There is a critical number of deposited NPs at a given power density of the laser so that the surface heating effect can allow the surface to reach a threshold temperature for the nucleation of surface bubbles. Furthermore, bubble nucleation on the BF surface is only possible if the incident laser frequency coincides with the surface plasmonic resonance peak of the NP since intense plasmonic heating is needed to generate a supercavitation—a necessity for optical pulling deposition.

ASSOCIATED CONTENT

Supporting Information

The Supporting Information is available free of charge at https://pubs.acs.org/doi/10.1021/acs.nanolett.0c04913.

Surface bubble nucleation by optical pulling force (MP4)

Surface bubble nucleation by optical pushing force-(MP4)

CS NPs deposition by optical pulling force (MP4)

CS NPs deposition by optical pushing force (AVI)

Laser focusing on BF surface in solid NP suspension (AVI)

Laser focusing on FF surface in solid NP suspension (AVI)

Methods; characterizing the CS NP deposition and surface bubble nucleation processes; finite element thermofluidic simulations details; Monte Carlo-assisted surface temperature field and heat flux simulations; and numerical simulations on the numerical aperture of objective lens (PDF)

AUTHOR INFORMATION

Corresponding Authors

Eungkyu Lee − *Department of Electronic Engineering, Kyung Hee University, Yongin-si, Gyeonggi-do 17104, Republic of Korea;* orcid.org/0000-0002-0211-0727; Email: eleest@khu.ac.kr

Tengfei Luo − *Department of Aerospace and Mechanical Engineering, University of Notre Dame, Notre Dame, Indiana 46556, United States; Department of Chemical and Biomolecular Engineering and Center for Sustainable Energy of Notre Dame (ND Energy), University of Notre Dame, Notre Dame, Indiana 46556, United States;* orcid.org/0000-0003-3940-8786; Email: tluo@nd.edu

Authors

Qiushi Zhang − *Department of Aerospace and Mechanical Engineering, University of Notre Dame, Notre Dame, Indiana 46556, United States;* orcid.org/0000-0003-1313-7965

Ruiyang Li − *Department of Aerospace and Mechanical Engineering, University of Notre Dame, Notre Dame, Indiana 46556, United States*

Complete contact information is available at: https://pubs.acs.org/10.1021/acs.nanolett.0c04913

Author Contributions

Q.Z., E.L., and T.L. designed the experiments, and Q.Z. set up the experiments. Q.Z. performed the experiment. Q.Z., R.L., E.L., and T.L. designed the simulations and Q.Z. performed the simulations. Q.Z. wrote the manuscript, R.L., E.L., and T.L. revised it.

Notes

The authors declare no competing financial interest.

ACKNOWLEDGMENTS

This work is supported by National Science Foundation (1706039) and the Center for the Advancement of Science in Space (GA-2018-268). T.L. would also like to thank the support from the Dorini Family endowed professorship in energy studies. This work is supported by the National Research Foundation of Korea (NRF) grant funded by the Korea government (MSIT) (No. NRF-2021R1C1C1006251). We also appreciate the partial supports from Notre Dame Integrated Imaging Facility (NDIF).

REFERENCES

(1) Prakash, M.; Gershenfeld, N. Microfluidic Bubble Logic. *Science* **2007**, *315* (5813), 832−835.

(2) Neumann, O.; Urban, A. S.; Day, J.; Lal, S.; Nordlander, P.; Halas, N. J. Solar Vapor Generation Enabled by Nanoparticles. *ACS Nano* **2013**, *7* (1), 42−49.

(3) Fang, Z.; Zhen, Y.-R.; Neumann, O.; Polman, A.; García de Abajo, F. J.; Nordlander, P.; Halas, N. J. Evolution of Light-Induced Vapor Generation at a Liquid-Immersed Metallic Nanoparticle. *Nano Lett.* **2013**, *13* (4), 1736−1742.

(4) Dongare, P. D.; Alabastri, A.; Neumann, O.; Nordlander, P.; Halas, N. J. Solar Thermal Desalination as a Nonlinear Optical Process. *Proc. Natl. Acad. Sci. U. S. A.* **2019**, *116* (27), 13182−13187.
(5) Hirsch, L. R.; Stafford, R. J.; Bankson, J. A.; Sershen, S. R.; Rivera, B.; Price, R. E.; Hazle, J. D.; Halas, N. J.; West, J. L. Nanoshell-Mediated near-Infrared Thermal Therapy of Tumors under Magnetic Resonance Guidance. *Proc. Natl. Acad. Sci. U. S. A.* **2003**, *100* (23), 13549−13554.
(6) Lukianova-Hleb, E. Y.; Ren, X.; Zasadzinski, J. A.; Wu, X.; Lapotko, D. O. Plasmonic Nanobubbles Enhance Efficacy and Selectivity of Chemotherapy against Drug-Resistant Cancer Cells. *Adv. Mater.* **2012**, *24* (28), 3831−3837.
(7) Baffou, G.; Quidant, R. Thermo-Plasmonics: Using Metallic Nanostructures as Nano-Sources of Heat. *Laser & Photonics Reviews* **2013**, *7* (2), 171−187.
(8) Liu, H.-L.; Fan, C.-H.; Ting, C.-Y.; Yeh, C.-K. Combining Microbubbles and Ultrasound for Drug Delivery to Brain Tumors: Current Progress and Overview. *Theranostics* **2014**, *4* (4), 432−444.
(9) Minai, L.; Hamra, M.; Yelin, D. Plasmonic Targeting of Cancer Cells in a Three-Dimensional Natural Hydrogel. *Nanoscale* **2018**, *10* (37), 17807−17813.
(10) Adleman, J. R.; Boyd, D. A.; Goodwin, D. G.; Psaltis, D. Heterogenous Catalysis Mediated by Plasmon Heating. *Nano Lett.* **2009**, *9* (12), 4417−4423.
(11) Baffou, G.; Polleux, J.; Rigneault, H.; Monneret, S. Super-Heating and Micro-Bubble Generation around Plasmonic Nanoparticles under Cw Illumination. *J. Phys. Chem. C* **2014**, *118* (9), 4890−4898.
(12) Sarhan, R. M.; Koopman, W.; Schuetz, R.; Schmid, T.; Liebig, F.; Koetz, J.; Bargheer, M. The Importance of Plasmonic Heating for the Plasmon-Driven Photodimerization of 4-Nitrothiophenol. *Sci. Rep.* **2019**, *9* (1), 3060.
(13) Zhao, Y.; Zhang, H.; Liu, Y.; Yang, Y.; Yu, L.; Xia, L.; Song, P. Effect of Reaction Conditions on the Characterization of Plasmon-Driven Surface Catalytic Reduction Reaction for Para-Nitroaniline in a Liquid Condition. *Plasmonics* **2020**, *15* (1), 31−37.
(14) Moon, S.; Zhang, Q.; Huang, D.; Senapati, S.; Chang, H.-C.; Lee, E.; Luo, T. Biocompatible Direct Deposition of Functionalized Nanoparticles Using Shrinking Surface Plasmonic Bubble. *Adv. Mater. Interfaces* **2020**, *7* (16), 2000597.
(15) Zhao, C.; Xie, Y.; Mao, Z.; Zhao, Y.; Rufo, J.; Yang, S.; Guo, F.; Mai, J. D.; Huang, T. J. Theory and Experiment on Particle Trapping and Manipulation via Optothermally Generated Bubbles. *Lab Chip* **2014**, *14* (2), 384−391.
(16) Ohannesian, N.; Li, J.; Misbah, I.; Zhao, F.; Shih, W.-C. Directed Concentrating of Micro-/Nanoparticles via Near-Infrared Laser Generated Plasmonic Microbubbles. *ACS Omega* **2020**, *5* (50), 32481−32489.
(17) Angelsky, O. V.; Bekshaev, A. Y.; Maksimyak, P. P.; Maksimyak, A. P.; Hanson, S. G.; Kontush, S. M. Controllable Generation and Manipulation of Micro-Bubbles in Water with Absorptive Colloid Particles by CW Laser Radiation. *Opt. Express* **2017**, *25* (5), 5232−5243.
(18) Ghosh, S.; Ranjan, A. D.; Das, S.; Sen, R.; Roy, B.; Roy, S.; Banerjee, A. Directed Self-Assembly Driven Mesoscale Lithography Using Laser-Induced and Manipulated Microbubbles: Complex Architectures and Diverse Applications. *Nano Lett.* **2021**, *21* (1), 10−25.
(19) Fujii, S.; Fukano, R.; Hayami, Y.; Ozawa, H.; Muneyuki, E.; Kitamura, N.; Haga, M. Simultaneous Formation and Spatial Patterning of ZnO on ITO Surfaces by Local Laser-Induced Generation of Microbubbles in Aqueous Solutions of $[Zn(NH_3)_4]^{2+}$. *ACS Appl. Mater. Interfaces* **2017**, *9* (9), 8413−8419.
(20) Zheng, Y.; Liu, H.; Wang, Y.; Zhu, C.; Wang, S.; Cao, J.; Zhu, S. Accumulating Microparticles and Direct-Writing Micropatterns Using a Continuous-Wave Laser-Induced Vapor Bubble. *Lab Chip* **2011**, *11* (22), 3816−3820.
(21) Armon, N.; Greenberg, E.; Layani, M.; Rosen, Y. S.; Magdassi, S.; Shpaisman, H. Continuous Nanoparticle Assembly by a Modulated Photo-Induced Microbubble for Fabrication of Micrometric Conductive Patterns. *ACS Appl. Mater. Interfaces* **2017**, *9* (50), 44214−44221.
(22) Ritchie, R. H. Plasma Losses by Fast Electrons in Thin Films. *Phys. Rev.* **1957**, *106* (5), 874−881.
(23) Polman, A.; Atwater, H. A. Plasmonics: Optics at the Nanoscale. *Mater. Today* **2005**, *8* (1), 56.
(24) Neumann, O.; Feronti, C.; Neumann, A. D.; Dong, A.; Schell, K.; Lu, B.; Kim, E.; Quinn, M.; Thompson, S.; Grady, N.; Nordlander, P.; Oden, M.; Halas, N. J. Compact Solar Autoclave Based on Steam Generation Using Broadband Light-Harvesting Nanoparticles. *Proc. Natl. Acad. Sci. U. S. A.* **2013**, *110* (29), 11677−11681.
(25) Yu, D.-M.; Liu, Y.-N.; Pan, X.-M.; Sheng, X.-Q. Accurate and Efficient Simulation of Plasmonic Bubbles Produced by Light Illumination. *2017 International Applied Computational Electromagnetics Society Symposium (ACES)* **2017**, 1−2.
(26) Wang, Y.; Zaytsev, M. E.; The, H. L.; Eijkel, J. C. T.; Zandvliet, H. J. W.; Zhang, X.; Lohse, D. Vapor and Gas-Bubble Growth Dynamics around Laser-Irradiated, Water-Immersed Plasmonic Nanoparticles. *ACS Nano* **2017**, *11* (2), 2045−2051.
(27) Tantussi, F.; Messina, G. C.; Capozza, R.; Dipalo, M.; Lovato, L.; De Angelis, F. Long-Range Capture and Delivery of Water-Dispersed Nano-Objects by Microbubbles Generated on 3D Plasmonic Surfaces. *ACS Nano* **2018**, *12* (5), 4116−4122.
(28) Liu, X.; Bao, L.; Dipalo, M.; De Angelis, F.; Zhang, X. Formation and Dissolution of Microbubbles on Highly-Ordered Plasmonic Nanopillar Arrays. *Sci. Rep.* **2016**, *5* (1), 18515.
(29) Zhang, Q.; Neal, R. D.; Huang, D.; Neretina, S.; Lee, E.; Luo, T. Surface Bubble Growth in Plasmonic Nanoparticle Suspension. *ACS Appl. Mater. Interfaces* **2020**, *12* (23), 26680−26687.
(30) Zhang, Q.; Pang, Y.; Schiffbauer, J.; Jemcov, A.; Chang, H.-C.; Lee, E.; Luo, T. Light-Guided Surface Plasmonic Bubble Movement via Contact Line De-Pinning by In-Situ Deposited Plasmonic Nanoparticle Heating. *ACS Appl. Mater. Interfaces* **2019**, *11* (51), 48525−48532.
(31) Wang, Y.; Zaytsev, M. E.; Lajoinie, G.; The, H. L.; Eijkel, J. C. T.; van den Berg, A.; Versluis, M.; Weckhuysen, B. M.; Zhang, X.; Zandvliet, H. J. W.; Lohse, D. Giant and Explosive Plasmonic Bubbles by Delayed Nucleation. *Proc. Natl. Acad. Sci. U. S. A.* **2018**, *115* (30), 7676−7681.
(32) Namura, K.; Shimada, Y.; Okai, S.; Kumar, S.; Suzuki, M. Thermoplasmonics for Investigation of Microbubble Dynamics in Degassed Water. *In Plasmonics: Design, Materials, Fabrication, Characterization, and Applications XVII; International Society for Optics and Photonics* **2019**, 110820S.
(33) Li, X.; Wang, Y.; Zaytsev, M. E.; Lajoinie, G.; Le The, H.; Bomer, J. G.; Eijkel, J. C. T.; Zandvliet, H. J. W.; Zhang, X.; Lohse, D. Plasmonic Bubble Nucleation and Growth in Water: Effect of Dissolved Air. *J. Phys. Chem. C* **2019**, *123* (38), 23586−23593.
(34) Detert, M.; Zeng, B.; Wang, Y.; Le The, H.; Zandvliet, H. J. W.; Lohse, D. Plasmonic Bubble Nucleation in Binary Liquids. *J. Phys. Chem. C* **2020**, *124* (4), 2591−2597.
(35) Chen, J.; Saklayen, N.; Courvoisier, S.; Shen, Z.; Lu, J.; Ni, X.; Mazur, E. Dynamics of Transient Microbubbles Generated by Fs-Laser Irradiation of Plasmonic Micropyramids. *Appl. Phys. Lett.* **2017**, *110* (15), 153102.
(36) Zou, A.; Gupta, M.; Maroo, S. C. Origin, Evolution, and Movement of Microlayer in Pool Boiling. *J. Phys. Chem. Lett.* **2018**, *9* (14), 3863−3869.
(37) Namura, K.; Nakajima, K.; Suzuki, M. Investigation of Transition from Thermal- to Solutal-Marangoni Flow in Dilute Alcohol/Water Mixtures Using Nano-Plasmonic Heaters. *Nanotechnology* **2018**, *29* (6), 065201.
(38) Namura, K.; Nakajima, K.; Kimura, K.; Suzuki, M. Photothermally Controlled Marangoni Flow around a Micro Bubble. *Appl. Phys. Lett.* **2015**, *106* (4), 043101.
(39) Xie, Y.; Zhao, C. An Optothermally Generated Surface Bubble and Its Applications. *Nanoscale* **2017**, *9* (20), 6622−6631.

https://doi.org/10.1021/acs.nanolett.0c04913
Nano Lett. XXXX, XXX, XXX−XXX

(40) Karim, F.; Vasquez, E. S.; Sun, Y.; Zhao, C. Optothermal Microbubble Assisted Manufacturing of Nanogap-Rich Structures for Active Chemical Sensing. *Nanoscale* **2019**, *11* (43), 20589−20597.
(41) Karim, F.; Vasquez, E. S.; Zhao, C. Fabricated Nanogap-Rich Plasmonic Nanostructures through an Optothermal Surface Bubble in a Droplet. *Opt. Lett.* **2018**, *43* (2), 334−336.
(42) Lin, L.; Peng, X.; Mao, Z.; Li, W.; Yogeesh, M. N.; Rajeeva, B. B.; Perillo, E. P.; Dunn, A. K.; Akinwande, D.; Zheng, Y. Bubble-Pen Lithography. *Nano Lett.* **2016**, *16* (1), 701−708.
(43) Lee, E.; Luo, T. Long-Distance Optical Pulling of Nanoparticle in a Low Index Cavity Using a Single Plane Wave. *Sci. Adv.* **2020**, *6* (21), No. eaaz3646.
(44) Lee, E.; Huang, D.; Luo, T. Ballistic Supercavitating Nano Swimmer Driven by Single Gaussian Beam Optical Pushing and Pulling Forces. *Nat. Commun.* **2020**, *11* (1), 2404.
(45) Huang, D.; Schiffbauer, J.; Lee, E.; Luo, T. Ballistic Brownian Motion of Supercavitating Nanoparticles. *Phys. Rev. E: Stat. Phys., Plasmas, Fluids, Relat. Interdiscip. Top.* **2021**, *103* (4), 042104.
(46) Lukianova-Hleb, E.; Hu, Y.; Latterini, L.; Tarpani, L.; Lee, S.; Drezek, R. A.; Hafner, J. H.; Lapotko, D. O. Plasmonic Nanobubbles as Transient Vapor Nanobubbles Generated around Plasmonic Nanoparticles. *ACS Nano* **2010**, *4* (4), 2109−2123.
(47) Boulais, É.; Lachaine, R.; Meunier, M. Plasma Mediated Off-Resonance Plasmonic Enhanced Ultrafast Laser-Induced Nanocavitation. *Nano Lett.* **2012**, *12* (9), 4763−4769.
(48) Lukianova-Hleb, E. Y.; Volkov, A. N.; Lapotko, D. O. Laser Pulse Duration Is Critical For the Generation of Plasmonic Nanobubbles. *Langmuir* **2014**, *30* (25), 7425−7434.
(49) Metwally, K.; Mensah, S.; Baffou, G. Fluence Threshold for Photothermal Bubble Generation Using Plasmonic Nanoparticles. *J. Phys. Chem. C* **2015**, *119* (51), 28586−28596.
(50) Lachaine, R.; Boutopoulos, C.; Lajoie, P.-Y.; Boulais, É.; Meunier, M. Rational Design of Plasmonic Nanoparticles for Enhanced Cavitation and Cell Perforation. *Nano Lett.* **2016**, *16* (5), 3187−3194.
(51) Maheshwari, S.; van der Hoef, M.; Prosperetti, A.; Lohse, D. Dynamics of Formation of a Vapor Nanobubble Around a Heated Nanoparticle. *J. Phys. Chem. C* **2018**, *122* (36), 20571−20580.
(52) Lapotko, D. Plasmonic Nanoparticle-Generated Photothermal Bubbles and Their Biomedical Applications. *Nanomedicine* **2009**, *4* (7), 813−845.

https://doi.org/10.1021/acs.nanolett.0c04913
Nano Lett. XXXX, XXX, XXX−XXX